Title: Impact of *Salmonella* genome rearrangement on gene expression

Authors and Affiliations

Emma V. Waters[1], Liam A. Tucker[1], Jana K. Ahmed [2], John Wain[1,3], Gemma C. Langridge[1*]

* Corresponding author. E-mail gemma.langridge@quadram.ac.uk; Telephone +44 (0)1603 255378

1 Microbes in the Food Chain, Quadram Institute Bioscience, Norwich Research Park, Norwich NR4 7UQ, United Kingdom;

2 The Wellcome Trust Sanger Institute, Wellcome Trust Genome Campus, Hinxton, Cambridge CB10 1SA, United Kingdom;

3 Norwich Medical School, University of East Anglia, Norwich Research Park, Norwich NR4 7TJ, United Kingdom

Running Title: Long-read sequencing determines GS, RNA shows impact of GS

Key Words: 48-plex Long-Read Sequencing; Genome Structure; RNAseq

Abstract

In addition to nucleotide variation, many bacteria also undergo changes at a much larger scale via rearrangement of their genome structure around long repeat sequences. These rearrangements result in genome fragments shifting position and/or orientation in the genome without necessarily affecting the underlying nucleotide sequence. To date, scalable techniques have not been applied to genome structure (GS) identification, so it remains unclear how extensive this variation is and the extent of its impact upon gene expression. However, the emergence of multiplexed, long-read sequencing overcomes the scale problem, as reads of several thousand bases are routinely produced that can span long repeat sequences to identify the flanking chromosomal DNA, allowing GS identification. Genome rearrangements were generated in *Salmonella enterica* serovar Typhi through long-term culture at ambient temperature. Colonies with rearrangements were identified via long-range PCR and subjected to long-read nanopore sequencing to confirm genome variation. Four rearrangements were investigated for differential gene expression using transcriptomics. All isolates with changes in genome arrangement relative to the parent strain were accompanied by changes in gene expression. Rearrangements with similar fragment movements demonstrated similar changes in gene expression. The most extreme rearrangement caused a large imbalance between the origin and terminus of replication and was associated with differential gene expression as a factor of distance moved towards or away from the origin of replication. Genome structure variation may provide a mechanism through which bacteria can quickly adapt to new environments and warrants routine assessment alongside traditional nucleotide level measures of variation.

Introduction

Small nucleotide-level variations in bacterial genomes, such as single-nucleotide polymorphisms (SNPs), or small insertions and deletions (indels) can have huge effects, from altering antibiotic resistance to switching entire metabolic pathways on or off. Bacteria can also undergo changes at a much larger scale via chromosomal rearrangements, where large genome fragments shift position and orientation in the genome to ultimately produce different unique genome structures (GSs) without affecting the underlying nucleotide sequence. These large structural variations occur via homologous recombination around long repeat sequences, including transposases (Achaz et al. 2002), duplicated genes (Nakagawa et al. 2003), prophages (Brüssow et al. 2004; Fitzgerald et al. 2021), insertion sequence (IS) elements (Darling et al. 2008; Weigand et al. 2019, 2017; Lee et al. 2016) and ribosomal operons (Liu and Sanderson 1998; Page et al. 2020). Independent to the repeat sequence used as anchor points, large chromosomal rearrangements have been associated with speciation, diversification, outbreaks, immune evasion and host/environmental adaptation in bacteria (Hughes 2000; Fitzgerald et al. 2021; Brüssow et al. 2004). Such variation could offer several advantages for the survival of bacteria: it may rapidly provide varying phenotypes to enhance adaptability between different niches, it is reversible, and can alter expression patterns of many genes (Hughes 2000). Unlike other types of repeat sequences, ribosomal operons are present in all bacterial genomes and therefore genomic rearrangement is a mode of variation possible in all bacteria with two or more ribosomal operons (Page et al. 2020).

Short-read whole genome sequencing (SRS), alongside the ability to multiplex samples, has provided the necessary resolution and high-throughput required to regularly identify SNPs and other small nucleotide changes in bacterial species important in human health. However, whilst highly accurate, SRS reads are only hundreds of base pairs long and are therefore unable to resolve long repeat sequences to produce a complete assembly or detect genomic rearrangement. Historically, the detection of GS variation has been challenging and performed on an ad hoc basis with lower

77 resolution methods such as long-range PCR or restriction enzyme digestion followed by pulsed-field
78 gel electrophoresis (PFGE) (Liu and Sanderson 1996; Kothapalli et al. 2005; Matthews et al. 2011).
79
80 The emergence of long-read sequencing (LRS) technologies from Pacific Biosciences and Oxford
81 Nanopore Technology (ONT) turns this situation around. LRS routinely produces reads of tens of
82 thousands bases long, with potential to span across repeat sequences into the flanking DNA,
83 producing complete assemblies that should ultimately allow the identification of GSs. The use of
84 comparative genomic methods alongside visualisation programs has enabled multiple genomes to
85 be aligned and compared which has helped highlight GS variation (Blom et al. 2016; Weigand et al.
86 2019; Fitzgerald et al. 2021; Darling et al. 2010) but investigating this variation using such methods is
87 challenging to perform at high-throughput due to compute power requirements.
88
89 With more complete bacterial genomes being deposited into public databases, we previously
90 demonstrated the ability to routinely identify GS variation from complete assemblies by developing
91 a software tool called *socru* (Page et al. 2020). With *socru* we reported that many bacterial species
92 important in human health display a wide range of GSs. The role GS variation plays in diseases may
93 be underappreciated due to the lack of high-throughput methods required to routinely assess this
94 variation.
95
96 Here we present the first use of LRS (via MinION, ONT) to confirm GSs originally identified by long-
97 range PCR and show multiplexed LRS can be used to routinely monitor and determine GSs in a high-
98 throughput manner. Our model system was *Salmonella enterica* serovar Typhi (*S*. Typhi), the
99 causative agent of typhoid fever, a pathogen in which GS variation has been repeatedly observed
100 (Liu and Sanderson 1996; Kothapalli et al. 2005; Liu and Sanderson 1998). *S.* Typhi appears
101 particularly capable of producing different GSs (Liu and Sanderson 1998; Matthews et al. 2011); with
102 more GSs found in *S.* Typhi than in all other *S. enterica* combined (Page et al. 2020). 45 GSs have

been identified in *S*. Typhi via lab-based methods (Kothapalli et al. 2005; Matthews et al. 2011) and in 2019, we identified 17 GSs using *socru* from a total of 112 publicly available complete genomes (Page et al. 2020), 4 of which were novel. The ability to identify GSs in large numbers of bacterial genome sequences allows us to address the question of biological relevance of this, very common, form of bacterial variation.

Here we have used long-term *in vitro* culture of a laboratory strain to generate rearrangements, confirming these with long-range PCR and LRS. With these stable GS defined strains we investigated the impact of genome rearrangement on growth phenotype and gene expression.

Results

Laboratory-generated genome structure variation

After 4 months of long-term static culture at ambient temperature, different-sized individual colonies of the parent *S.* Typhi strain (WT) were observed, indicative of different growth phenotypes (Supplemental Fig. S1A). Both large and small colonies were picked at random for analysis.

Genome structure by long-range PCR

To determine GSs of *S*. Typhi colonies via long-range PCR, 14 forward and reverse primers were designed (Supplemental Table S1) to bind to regions 100-900 bp downstream of the *rrs* gene and upstream of the *rrf* gene of each of the seven *rrn* operons, respectively. These primers were used to perform 91 individual long-range PCRs to test all possible combinations of neighbouring fragments. Primer combinations which amplified across an entire *rrn* operon produced a ~6 kb band. The presence of seven different PCR products of correct sizes (~6 kb) confirmed WT derivatives had seven genomic fragments and allowed their GSs to be determined (Fig. 1, Table 1 and Supplemental Fig. S2). WT itself was derived from Ty2 (see Methods) and confirmed to have the same GS 2.66 (17'35642') (genome accession GCF_000007545.1.) (Deng et al. 2003).

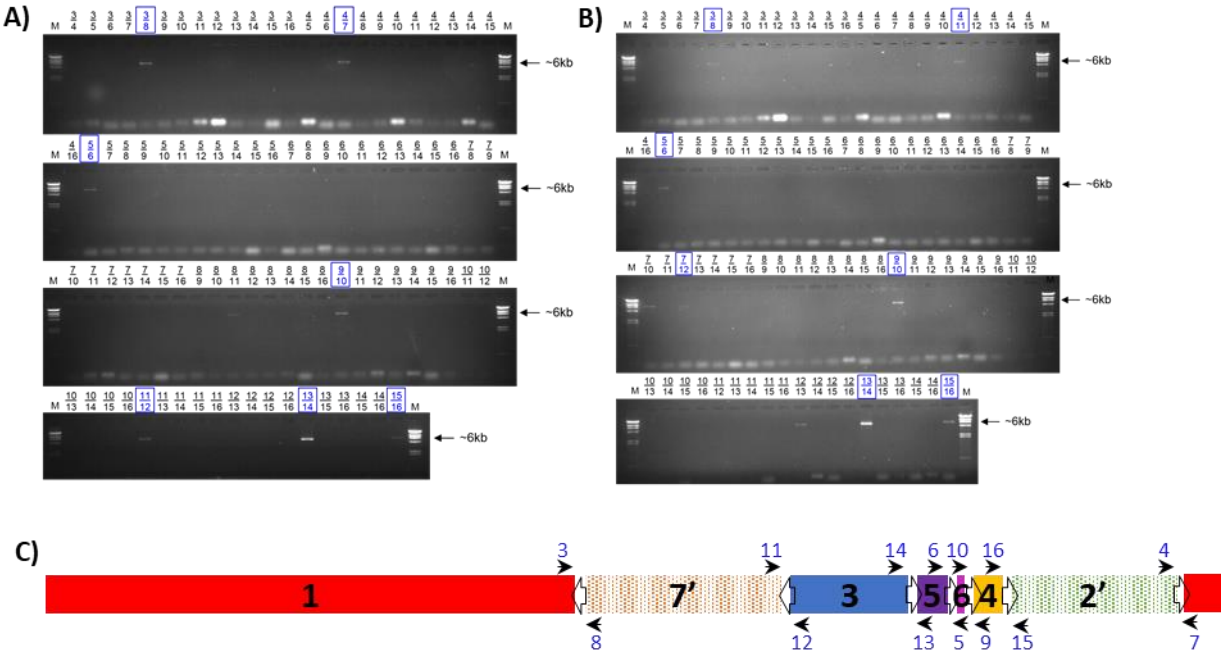

Figure 1. Long-range PCR for genome structure determination. Gel images of long-range PCR products of WT derivatives 7 (*A*) and T (*B*). Primer combinations are given above every well. Combinations indicated in blue boxes lead to the conclusion of the respective GS for that isolate. (*C*) Illustration of the primer binding sites within the *Salmonella* genome (Ty2 (WT) GS2.66, 17'35642'). Open arrows indicate the *rrn* operons and their orientation; black arrows indicate the direction and location of the primers numbered in blue; black numbers denote genome fragments.

Variant	Informative products	Non-informative products	Genome arrangement
7	3/8, 4/7, 5/6, 9/10, 11/12, 13/14, 15/16	3/5, 8/11*	17'35642' (GS2.66)
8	3/8, 4/7, 5/6, 9/12, 10/11, 13/14, 15/16	6/13*, 8/11*	1'24'3567 (GS19.9)
U	3/8, 5/6, 11/14, 12/13, 15/16	8/11*	1'24'6'5'37 (GS2.57)
T	3/8, 4/11, 5/6, 7/10, 7/12, 9/10, 12/13, 13/14, 15/16		135642'7 (GS21.3) and 1'6'5'35642'7**

Table 1. Arrangements determined by long-range PCR. Primer combinations resulting in PCR products that gave an informative 6 kb band were used to determine genome structures. Primer combination products were deemed non-informative either due to spurious bands of incorrect size or representing circularised fragments. *8/11 = circularised fragment 6, 6/13 = circularised fragment 5; **no GS assigned because the structure includes duplicated fragments.

Long-range PCR of variant 7 produced eight amplified PCR products of the correct size (Fig. 1A). The amplification of primer combination 8/11 represented the circularised fragment 6. The other seven bands indicated which fragments neighboured each other and demonstrated that isolate 7 maintained the parental GS described by 17'35642' (GS 2.66, Fig. 2). Variant 8 produced nine amplified PCR products of 6 kb in length (Supplemental Fig. S2A) representing 1'24'3567 (GS19.9),

where fragments 3, 5 and 6 had all undergone inversion in comparison to the parental GS (Fig. 2). Variant U produced five amplified PCR products of 6 kb in length (Supplemental Fig. S2B). These confirmed fragments 65'371' [=1'735'6] and fragments 24' were located together, respectively. Only one valid orientation existed for these two fragment blocks in relation to each other, as ribosomal operon direction must follow the direction of replication (Page et al. 2020). This gave the rearranged structure 1'24'6'5'37 (GS2.57), where fragment 3 has an inverted orientation in comparison to the parental GS (Fig. 2).

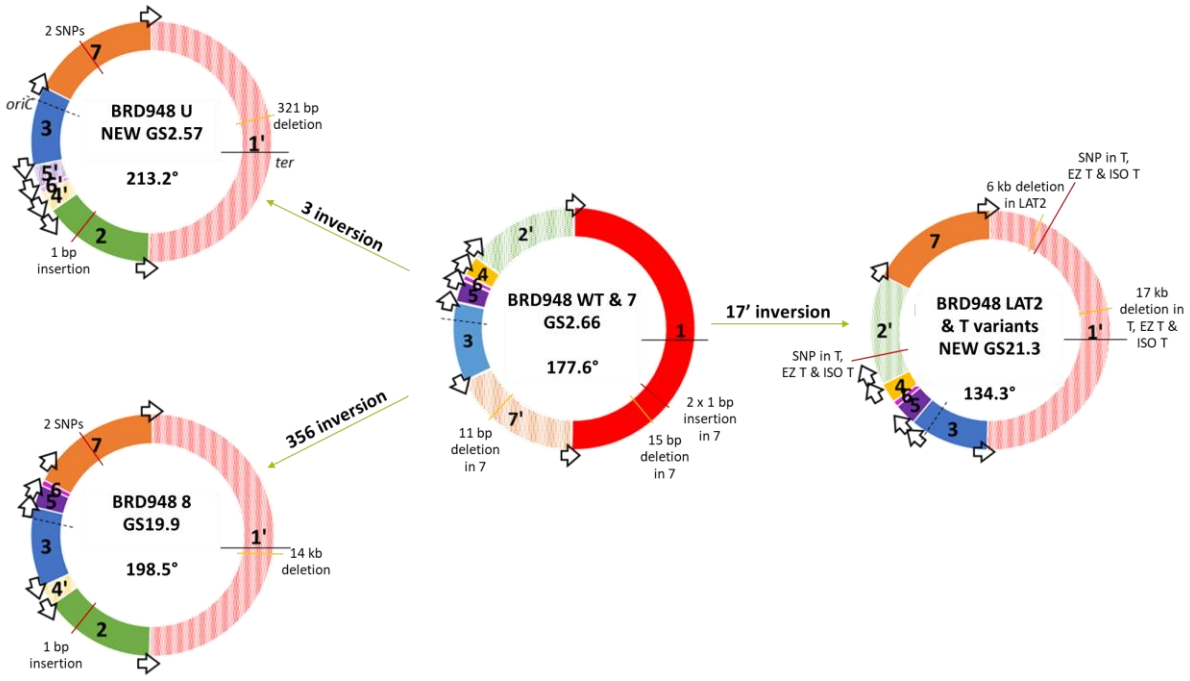

Figure 2. Genome rearrangements of variants relative to WT. Schematic showing variant genome structures (GSs) and the rearrangement of WT fragments required to achieve these. GS fragments are labelled in respect to the *Salmonella* enterica database reference LT2 (genome accession GCF_000006945.2) and drawn beginning with the largest fragment and working in a clockwise fashion around the chromosome. The fragment containing origin of replication (here fragment 3) has its orientation fixed to match the orientation of the database reference and therefore inversion of fragment 3 is depicted as the rest of the chromosome inverted. Inverted fragment orientations are denoted prime (') with striped colours. *Ori-ter* balance is given in degrees for each GS, going clockwise from *ter* to *oriC* as drawn. Arrows: ribosomal operons; *oriC* and dashed lines: origin of replication; and *ter* and black whole lines: terminus of replication. Data from genome sequencing used to identify insertions (red lines) and deletions (yellow lines) in each variant in comparison to WT; bp, base pairs.

Long-range PCR of variant T produced nine amplified 6 kb PCR products (Fig. 1B). The informative bands indicated variant T displayed a potentially mixed GS population, with genome structures of

both 135642'7 (GS21.3) and 1'6'5'35642'7 being present. These GSs both had fragments 1 and 7' inverted relative to the parental GS (Fig. 2) and the latter had a duplication of fragments 5 and 6 within fragments 1 and 3.

These data confirmed the utility of long-range PCR in successfully identifying GS but also highlighted drawbacks for scalability e.g. requirement for 91 individual long-range PCRs (plus additional controls) to test all possible combinations of neighbouring fragments, and interpretation of the resulting gel to take into account informative versus spurious or misleading bands

Genome structure by long-read sequencing

Following > 10 years of storage at -80 ^{o}C, we re-cultured the parent strain and 4 variants, and performed LRS on these to determine if the GSs had remained stable and whether this method recapitulated the same GS as those identified by long-range PCR. For the parent strain and variants 7, 8 and U, DNA extraction was performed from over-night cultures. For variant T, overnight culture was repeatedly unsuccessful, and cells were instead harvested directly from an original glycerol stock prior to high molecular weight DNA extraction. We determined that 2.5x10^{5} cells/mL within this glycerol stock were still viable (Supplemental Fig. S3). Due to the limited amount of glycerol stock, trials at culturing this variant using alternative media (EZ-rich and iso-sensitest) were used to successfully revive T and make fresh glycerol stocks, named EZ T and ISO T respectively. For EZ T and ISO T, DNA extraction was performed accordingly from over-night cultures. All parent and variant DNA was sequenced on the MinION platform (ONT); long-read sequence data are presented in Table 2.

	Raw reads			Filtered reads				Assembly info		
Sample	Total reads	Read length N50 (bp)	Mean read length (bp)	Filtered reads	Read length N50 (bp)	Mean read length (bp)	Coverage	Number of contigs	Total length (Mb)	Genome Structure

WT	93,987	15,251	8,019	78,814	15,435	9,352	154	1	4.8	GS 2.66 (17’35642’)
7	178,989	10,047	5,582	144,780	10,217	6,641	200	1	4.8	GS 2.66 (17’35642’)
U	136,394	10,030	4,954	101,078	10,386	6,355	134	1	4.8	GS2.57 (1’24’6’5’37)
8	361,660	8,161	4,968	303,526	8,290	5,686	360	1	4.8	GS19.9 (1’24’3567)
T	742,517	11,512	6,349	637,788	11,705	7,173	953	2	4.8	GS21.3 (1’35642’7) and 1’6’5’35642’7**
EZ T	229,085	16,020	8,228	193,979	16,212	9,512	383	4	4.8	1’6’5’35642’7^{+}
ISO T	546,089	15,857	9,036	485,918	15,952	9,983	1011	1	4.8	GS21.3 (1’35642’7) and 1’6’5’35642’7^{++}
LAT2	506,348	11,043	6,379	442,729	11,162	7,095	654	1	4.8	GS21.3 (1’35642’7)

Table 2. Long-read information from the WT parent strain and 7 derivatives. Filtered reads have length greater than 1 kb and min_mean_q of 50. Coverage based on length of Ty2 genome. **fragments 5 and 6 assembled on separate contig to rest of chromosome, mixed GS population; $^{+}$fragments 5 and 6 assembled on individual contigs, single GS population. $^{++}$all fragments assembled as single chromosomal contig, mixed GS population

Raw basecalled and demultiplexed fastq reads were filtered for high quality and for length greater than 1 kb. In our dataset, assemblies of the expected genome size were generated for all isolates. Genome structure assignments were determined from the assemblies using *socru* or prokka and Artemis Comparison Tool. Two isolates, U and T, have novel GSs not yet documented in the literature or public databases.

WT, 7, U and 8 each assembled into a single contig of ~4.8 Mb which gave identical GSs to those determined by long-range PCR (Fig. 2, Table 2). In contrast, long-read assembly of T was in two contigs: 4.6 Mb (fragments 1’, 3, 4, 2’ and 7) and 0.2Mb (fragments 6 and 5) with the latter having twice the coverage of the former (Supplemental Fig. S4). A similar situation was seen with EZ T where fragments 5 and 6 were present on two individual contigs but still at twice the coverage of the main contig. To investigate the potential of a mixed GS population of 1’6’5’35642’7 and 1’35642’7 in these isolates, we searched the filtered reads for those which spanned fragments 3 and 5 and fragments 5’ and 3 (Supplemental Material, Supplemental Fig. S5, Supplemental Table S2). For T, the 3-5 bridge was present at approximately twice the presence of the 5’-3 bridge (208:111)

indicating the two different GSs were present in roughly equal proportions and potentially explains why the assembly software struggled to either generate a complete assembly or assemble the dominant structure. For EZ T, the two bridges were present in approximately equal amounts (87:100), indicating the presence of 1'6'5'35642'7 only and the loss of GS21.3 from the population, in comparison to the original variant T. Assembly of ISO T gave a single contig of ~4.8 Mb with a genome structure of 1'35642'7 (GS21.3). However, the two bridges were found in the filtered reads at a ratio of 2:1 (305:165), suggesting the presence of both GSs, as observed for T.

Long-read sequencing as a method to monitor GS variation

Having confirmed LRS provided the same GS as long-range PCR, we used long-term culture in different media to generate genome rearrangements. Twelve large and small colonies were picked at random and processed for multiplexed LRS on a single MinION flowcell.

Sequencing was performed for up to 5 days to achieve the maximum amount of data for highest coverage, before data was demultiplexed and processed through our GS identification pipeline. Following LRS library preparation with the ONT rapid barcoding kit, assemblies of the expected genome size were generated for all tested colonies which had a mean read length of ~10 kb and minimum ~60x coverage. In one small, pin-prick colony (Supplemental Fig. S1B), LAT2, we observed genome rearrangement had occurred, producing a GS identical to isolate ISO T (1'35642'7, GS21.3) and was confirmed to contain only this GS via examination of filtered reads (Supplemental Table S2). The remaining colonies tested had not undergone rearrangement and had the parental GS.

Nucleotide-level variation

Additional short-read whole genome sequencing was performed to generate hybrid assemblies for parent strain WT and variants 7, 8, U, T, EZ T, ISO T and LAT2. These gold-standard hybrid assemblies

were evaluated with CheckM, which confirmed they were ≥ 99.66 % complete and contained <= 0.4 % contamination. The only exception to this was the completeness of T which was 93.07 %.

As expected, GS analysis of the hybrid assemblies gave identical results to those previously identified via long-read assemblies alone. Core genome SNP analysis of the variants confirmed that variants 7 and LAT2 were indistinguishable from the parent strain, WT. Isolates 8 and U were identical to each other but had 2 SNPs different to WT, at 4,629,839 bp (G→T) and 4,637,875 bp (C→A) in the Ty2 reference genome. T, EZ T and ISO T were identical to each other but harboured 2 different SNPs from WT: 677,285 bp (A→G) and 3,192,356 bp (C→T). All SNPs occurred in coding sequences, causing non-synonymous changes (Table 3). cgSNPs at 3,192,356 and 4,637,875 bp generated premature stop codons within the first and second domains of *tolC* and *treR* respectively. The SNP at 677,285 bp occurred in *rcsB* causing an amino acid located in the binding domain to change from a hydrophobic phenylalanine to a polar serine. The SNP at 4,629,839 bp occurs in t4482 (*licR*) and changes a negative charged aspartate to a large non-polar tyrosine.

Further comparative genomics with Breseq revealed additional nucleotide variation, particularly associated with fragment 1 (Fig. 2, Table 3). Breseq was unable to detect the duplicated fragments 5 and 6 which are seen in T, EZ T and ISO T, as previously mentioned. Using the different levels of variation seen in the isolates generated in this work, we have generated the most parsimonious lineage (Supplemental Fig. S6).

Sample	Type of nucleotide variation	Positions in Ty2 genome (bp)	Genes affected	Fragments affected
7	1 bp insertion (C)	964,704	n/a	1
	1 bp insertion (C)	964,743	n/a	1
	11 bp deletion	4,507,390 – 4,507,400	*tviA* (t4353)	7
	15 bp deletion	821,258 – 821,272	*baeR* (t0741)	1
8	1 SNP (G→T)	4,629,839	t4482	7
	1 SNP (C→A)	4,637,875	*treR* (t4490)	7
	1 bp insertion (A)	3,191,594	*tolC* (t0310)	2

	14 kb deletion	1,523,024 – 1,537,156	12 genes completely deleted (t1474-1487) (including *hlyE*, *osmC*, *rpsV*, *sfcA*, *adhP*, *smvA* and *narU*) and partial deletion of 2 genes (t1473 and *narZ* t1488)	1
U	1 SNP (G→T)	4,629,839	t4482	7
	1 SNP (C→A)	4,637,875	*treR* (t4490)	7
	1 bp insertion (A)	3,191,594	*tolC* (t0310)	2
	321 bp deletion	1,313,723 – 1,314,043	*lppB* (t1244)	1
T, EZ T and ISO T	1 SNP (A→G)	677,28	*rcsB* (t0595)	1
	1 SNP (C→T)	3,192,356	*tolC* (t0310)	2
	17 kb deletion	1,313,228 – 1,330,361	12 genes completely deleted (t1244-1257) (including *ippB*, *ippA*, *pykF*, *ttrA*, *ttrC*, *ttrB*, *ttrS*, *ttrR* and *ydhZ*) and partial deletion of 1 gene (t1258)	1
LAT2	6 kb deletion	598,923 – 605,161	4 genes completely deleted (t0527-0530) (including *ackA*) and partial deletion of 2 genes (t0526 and t0531) (including *pta* (t0526))	1

Table 3. Nucleotide variation. SNPs, insertions and deletions identified in the 7 variants in comparison to the WT parent.

Impact of genome rearrangement on *ori-ter* balance

All rearranged isolates generated by long-term growth showed additional nucleotide level variation with all displaying indels and all but LAT2 having SNPs. In all cases, except isolate 7, the rearrangement caused the *ori-ter* balance to become more imbalanced. All the indels, except the smallest of 321 bp seen in U, occurred in the longer replichore which may represent some mechanism of compensation towards restoring *ori-ter* balance (Fig. 2). However, deletions ranged in size from 6-17 kb only resulted in shifting this balance by a maximum of 0.5°.

Impact of genome rearrangement on growth rate

Variants 7, 8 and U showed similar growth phenotypes and colony sizes to the parent strain (Fig. 3, Supplemental Fig. S7). These growth phenotypes were consistent when repeated after 10 years in -80 °C storage (Supplemental Fig. S7). From initial growth experiments, isolate T showed a clear reduction in colony size (Supplemental Fig. S1A) and growth rate compared to the parent.

277 Subsequent growth experiments of revived T isolates and LAT2 showed similar reduction in colony
278 size and growth rate (Fig. 3, Supplemental Fig. S1B).
279

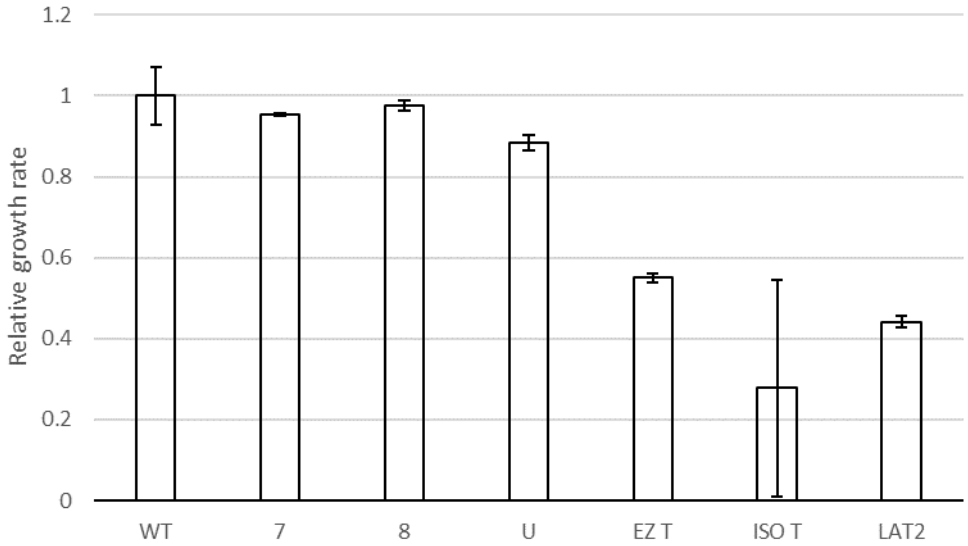

280

281 **Figure 3.** Growth rates of the 6 derivatives. Calculated for at least three independent biological replicates per
282 isolate, relative to the WT parent strain. Error bars indicate standard deviation.
283

284 **Impact of genome rearrangement on gene expression**

285 The impact of rearrangement was explored using RNAseq to identify differentially expressed genes
286 (DEGs). As T, EZ T, ISO T and LAT2 all had the same GS, with or without duplicated fragments,
287 RNAseq was performed on WT parental strain and variants 7, 8, U and LAT2. Differential expression
288 was determined for each variant in comparison to the parent strain, which harbours 4431 genes
289 (Supplemental Table S3).
290

291 Isolate 7 (GS2.66) showed 63 significant DEGs (Supplemental Table S4). Only 13 genes were
292 upregulated in isolate 7, which included the superoxide dismutase *sodA*, an indicator of oxidative
293 stress also known to be positively regulated by BaeRS (Guerrero et al. 2013). This raises the
294 possibility that the 15 bp in-frame lesion detected in *baeR*, whilst appearing within a response
295 regulator receiver domain (Pfam: PF00072), may not have a functional impact on BaeR activity. The
296 *cyo* genes encoding for the cytochrome *bo* (ubiquinol oxidase) terminal complex were also

297 upregulated. Genes involved in Vi antigen (the capsular polysaccharide of *S.* Typhi which is a major
298 virulence factor) and histidine biosynthesis were downregulated; the former may be partly due to
299 the lesion detected within *tviA* which caused a frameshift mutation (Table 3).
300
301 For isolate 8 (GS19.9) and isolate U (GS2.57), 68 and 131 significant DEGs were identified
302 respectively (Supplemental Table S4). Whilst representing different genome arrangements, they
303 shared the same inversion of fragment 3, with the additional inversion of 5 and 6 in isolate 8 (Fig. 2).
304 Not including the deletion of 14 genes in isolate 8, 83 % (45/54) of the significant DEGs in this isolate
305 were also observed in isolate U. This included the upregulation of trehalose transport and utilisation
306 (*treB*, *treC*) and of *ramA*, a transcriptional activator associated with multidrug resistance via AcrAB
307 efflux (Nikaido et al. 2008), though no differential expression was observed for *acrAB* for either
308 isolate. Tyrosine biosynthesis was downregulated in both (*tyrA*), as well as elements of
309 glycolysis/gluconeogenesis (*pgk*, *eno*), with additional genes *pfkA*, *ppc* and *fba* downregulated in U.
310
311 By far the greatest impact upon expression was observed in LAT2, where 758 DEGs were identified
312 (Supplemental Table S4). These were assessed in several ways: firstly, the genomic location of each
313 significant DEG was plotted against the genome arrangement of both the parent (GS2.66) and LAT2
314 (GS21.3) (Fig. 4). This indicated that for LAT2, genes on fragment 1 between the terminus and
315 fragment 3 appeared generally upregulated, coinciding with their shift of ~ 800 kb towards the origin
316 of replication. It also showed a general downregulation of genes on the other half of fragment 1
317 (between the terminus and fragment 7) in alignment with their shift of ~ 800 kb away from the
318 origin. Similarly, a general trend of downregulation was observed for fragment 7 genes, which had
319 shifted ~600 kb away from the origin.

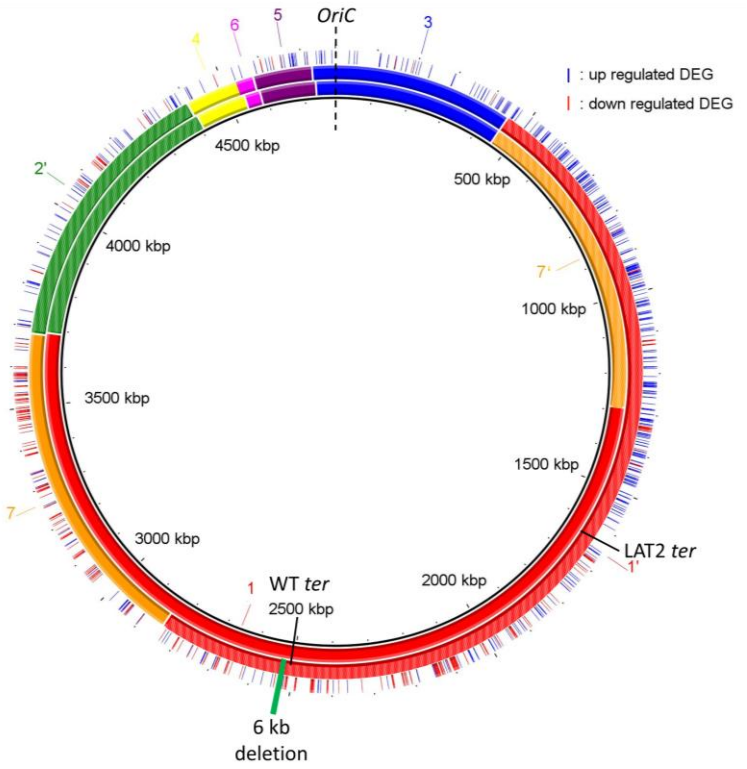

Figure 4. Gene expression in LAT2. BRIG representation of the WT genome (inner circle, GS 2.66 (17'35642')) and the LAT2 genome (middle circle, GS21.3 (1'35642'7)). Genome fragments are numbered and shown as coloured blocks, inverted fragments are coloured with stripes (e.g. green fragment 2) as per (Page et al. 2020). Same origin (*oriC*, dashed black line) and different termini (*ter*, solid black lines) of replication are shown for each genome. Outer circle shows location of up (blue line) and down (red line) regulated differentially expressed genes (DEG). Deletion event denoted in LAT2 by solid green rectangle.

We therefore plotted genes per fragment by the distance they had shifted from the origin. This confirmed a large proportion of significant DEGs were found at the extreme ends of fragment 1 (Fig. 5A), though no strong correlation between direction of regulation and distance shifted to/from origin was observed across the fragment (R^2 = 0.2836). For fragment 7, 81 % (99/122) of significant DEGs were downregulated (Fig. 5B).

We also investigated which clusters of orthologous gene (COG) functions were present in the significant DEGs (Fig. 5C). All but one of the genes (34/35) affecting cell motility (COG category N) were downregulated in LAT2. Conversely, genes in categories D – cell cycle control, I – lipid transport and metabolism and J – translation and ribosomal structure were almost all upregulated.

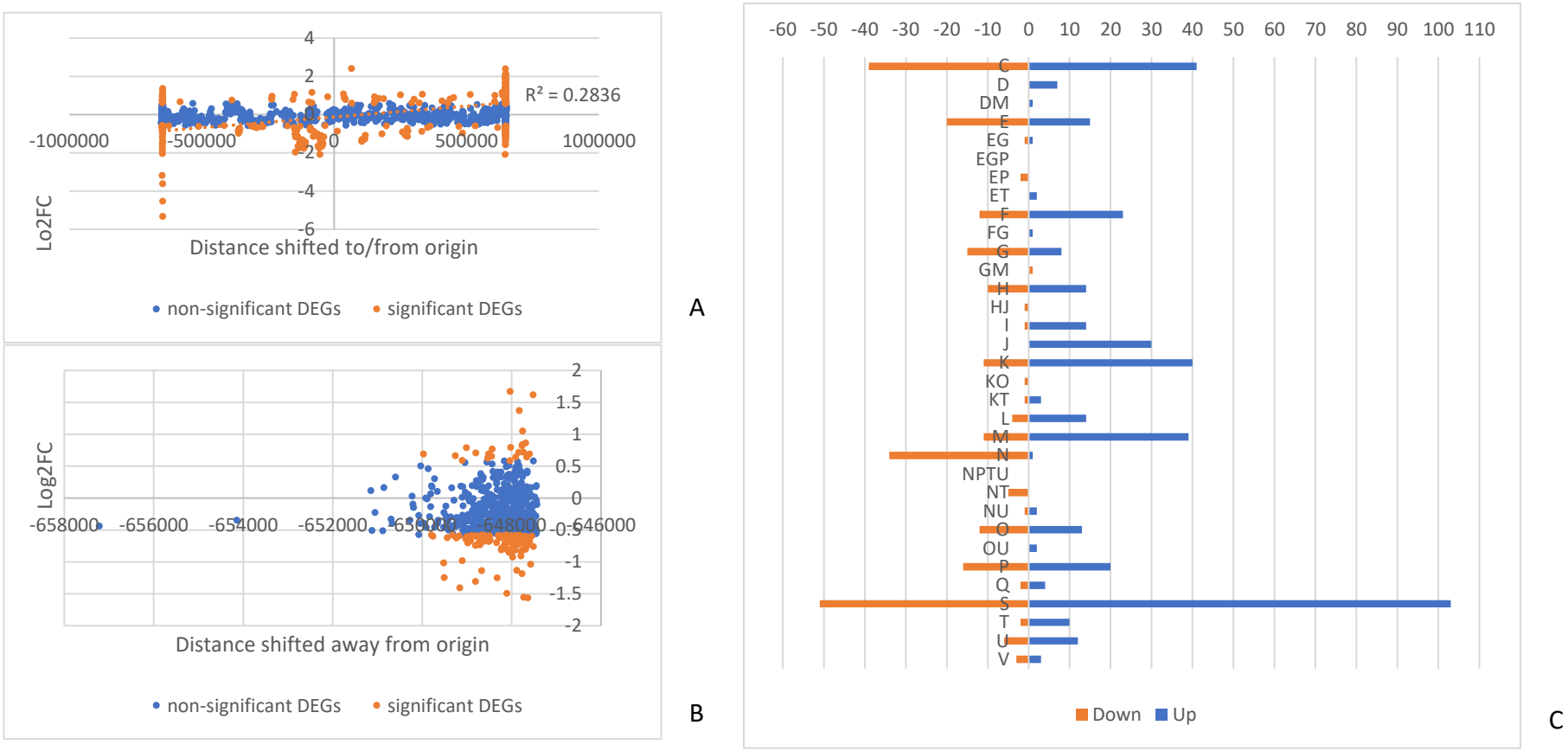

Figure 5. Impact of genome rearrangement on gene expression in LAT2. Graphical distribution of log2FC against distance a gene has moved towards or away from the origin of replication for LAT2 genes on (*A*) fragment 1 and (*B*) fragment 7. Genes coloured by non (blue) and -significance (orange). Linear correlation in (*A*) shown as orange dotted line. (*C*) Distribution of significant differentially expressed genes (DEGs) from LAT2 across COG categories. Down-regulated DEGs shown in orange, up-regulated in blue. COG categories: C Energy production and conversion; D Cell cycle control, cell division, chromosome partitioning; E Amino acid transport and metabolism; F Nucleotide transport and metabolism; G Carbohydrate transport and metabolism; H Coenzyme transport and metabolism; I Lipid transport and metabolism; J Translation, ribosomal structure and biogenesis; K Transcription; L Replication, recombination and repair; M Cell wall/membrane/envelope biogenesis; N Cell motility; O Posttranslational modification, protein turnover, chaperones; P Inorganic ion transport and metabolism; Q Secondary metabolites biosynthesis, transport and catabolism; S Function unknown; T Signal transduction mechanisms; U Intracellular trafficking, secretion, and vesicular transport; V Defense mechanisms.

Discussion

We have demonstrated that long-read sequencing can be used for GS identification, with the added benefit over long-range PCR of scalability alongside all the genetic information that comes from whole genome sequencing. We have shown that genome rearrangement has an impact on gene expression and growth rate with the greatest impact being when the *ori-ter* balance is most disturbed.

Considering that there are 1440 possible *S*. Typhi GS structures, it is of interest that the GS21.3 arrangement of T was recapitulated in an independent long-term growth experiment in isolate LAT2. This arrangement appears disadvantageous to bacterial growth due to the *ori-ter* balance being offset by ~45^{o} (Fig. 2), which was borne out in the growth rate analysis (Fig. 3). Theoretically, having fragments 1 and 3 next to each other in this arrangement of 1’35642’7 is the second most extreme *ori-ter* position that could be formed (the most extreme being where fragment 3 is also inverted: 1’3’5642’7). Even though isolates T and LAT2 were generated in different growth media, there are other conditions in common, including limited nutrients, growth waste products and anaerobic conditions. As such, we speculate that reduced growth rates seen in rearrangements such as GS21.3 may actually provide a selective advantage for survival in nutrient limited, or toxic, environments.

Given the growth effect of GS21.3, we investigated the impact that rearrangement had upon expression in all our GS arrangements. We observed that rearrangements with similar fragment movements demonstrated similar changes in gene expression. This was the case for isolates 8 and U which shared the inversion of fragment 3, and over 80 % of the DEGs in isolate 8 were also found in isolate U. In LAT2, GS21.3 caused a large imbalance between the origin and terminus of replication and was associated with differential gene expression as a factor of distance moved towards or away from the origin of replication, i.e. down regulation of most DEGs on fragment 7 and the greatest

number of up/down regulated DEGs being found at the extremes of fragment 1. Specific COG function analysis highlighted that the metabolically costly production of flagella for cell motility was down regulated in LAT2 (> 30 genes all located on fragment 1), highlighting that a change in genome arrangement could be providing a mechanism of adaptation to poor nutrient levels.

In addition to GS changes, DNA sequencing also revealed SNP variation and larger deletions of hundreds to thousands of base pairs. The SNPs observed all caused non-synonymous changes and mostly occurred in outer membrane proteins. In isolate T (and derivatives EZ T and ISO T), one SNP results in a premature stop codon in the middle of TolC (Guan et al. 2015), a key outer membrane component of several multidrug efflux pumps. The second SNP was in *rcsB*, a transcriptional regulator that responds to cell envelope stress (Wall et al. 2018) and positively regulates Vi antigen biosynthesis (Virlogeux et al. 1996), caused a non-synonymous change within the DNA binding domain (Casino et al. 2018). However, since neither of these SNPs were found in LAT2, their effect on expression in this unbalanced arrangement will be the subject of future investigation.

The two SNPs (t4482, a putative *licR*-type regulator and *treR*) and indel shared by isolates 8 and U, suggest a link between genomic and genetic events. The SNP in *treR* resulted in a premature stop codon between its two protein domains (Hars et al. 1998). TreR negatively regulates *treBC* - aligning with the de-repression of *treBC* in these variants which have been shown in *E. coli* to have a role in mitigating against low osmolarity, by increasing conversion of trehalose to glucose via trehalose-6-phosphate (Vanaporn and Titball 2020). The indel was earlier in the *tolC* sequence than the SNP in the T variants, sending the sequence out of frame after 10 amino acids, resulting in a premature stop codon after 43 aa. As all upstream sequence remained unchanged, this did not affect *tolC* expression. However, the loss of TolC function in three variants with GS changes, by independent lesions in at least two, suggests that the export capacities of its associated pumps can be deleterious under the low-nutrient conditions used here.

In all rearranged isolates (U, 8, T and LAT2), deletions relative to the parent strain were identified in fragment 1 (Fig. 2). Strikingly, the largest deletions (14 kb and 17 kb) were very close to the terminus of replication in 8 and T, respectively. In *Salmonella enterica*, Koskiniemi et al demonstrated that deletion rates are highest near the terminus of replication and may be a mechanism to increase fitness in the particular conditions under which deletion occurs (Koskiniemi et al. 2012). This raises the possibility that genome rearrangement is a mechanism to target deletions.

To support investigation of GSs, long-read technology is key, and it is continually evolving. At the beginning of our routine monitoring of GSs, only 12-plex kits for the MinION were available to perform this work in a higher throughput manner. In 2020, to coincide with rapid large scale Covid sequencing, ONT released a 96-plex ligation kit which was quickly taken on by the community to sequence 96 samples containing 1 kb amplicons at once (Tyson et al. 2020). This throughput can now be leveraged to sequence up to 96 bacterial genomes per flowcell (Arredondo-Alonso et al. 2021), making routine GS identification the most accessible it's ever been.

Conclusion

In this study, we have identified 2 novel GSs, with one (GS21.3) being observed on two independent occasions. Through genomic and transcriptomic analysis, we have shown that the impact of rearrangement affects gene expression in similar ways across similar structural changes whilst the genome remains relatively balanced between the origin and terminus of replication, with more dramatic expression changes occurring in an unbalanced arrangement, accompanied by reduced growth rate. We also note that rearrangement appears to occur in conjunction with additional nucleotide variation, especially affecting gene presence near the terminus of replication. Incorporating routine identification of GS via long read sequencing will increase our understanding

of the frequency of this type of variation and provide a strong foundation to systematically assess the role of rearrangement in bacterial adaptation.

Methods

Bacterial isolates included in this study

The *S*. Typhi strain used in these studies is WT, a long-term culture derivative of WT26 pHCM1 (Langridge et al. 2009). WT26 pHCM1 was originally derived from the attenuated Ty2-derived strain CVD908-*htrA*, which has deletion mutations in *aroC*, *aroD*, and *htrA* (Tacket et al. 1997), and further included a point mutation in *gyrA* and the multiple antibiotic resistance plasmid, pHCM1 (Turner et al. 2006). Long-term culture of WT26 lead to the loss of pHCM1 plasmid and the renaming of this strain to WT. Long-term, *in vitro* growth of WT in low salt LB (1 % tryptone, 0.5 % yeast, 0.5 % NaCl) generated 4 isolates (7, 8, U and T). After 10 years storage, isolate T was unable to be revived from glycerol stocks in original growth media and could only be revived using alternative media (EZ-rich (Teknova) and isosensitest (Oxoid)) which were used to make fresh glycerol stocks, named EZ T and ISO T respectively. Further long-term, *in vitro* growth of WT generated an isolate (LAT2) in isosensitest broth with a growth phenotype that deviated from that of the parent strain.

Growth conditions for generation of different genome structures with long-term, *in vitro* growth

Long-term cultures were used to induce *in vitro* genomic rearrangement in *S*. Typhi WT. Due to the nature of attenuation in this strain, WT requires media to be supplemented with aromatic amino acid mixture (aro-mix) of L-phenylalanine, L-tryptophan, and L-tyrosine at a final concentration of 40 µg/mL and 2, 3-dihydroxybenzoic acid and ρ-aminobenzoic acid at a final concentration of 10 µg/mL.

Generation of variants 7, 8, U and T was achieved by growing a 50 mL aro-mix supplemented low salt LB culture of WT overnight at 37 °C, 180 rpm before leaving to grow at room temperature. After 4

447 months, 50 µL was plated out on low salt LB agar (Supplemental Fig. S1A), supplemented with aro-
448 mix, and incubated at 37 °C for 48 hrs; individual colonies were picked for long-range PCR.
449
450 Generation of variant LAT2 and the other colonies tested by MinION sequencing was carried out as
451 above and also extended to include aro-mix supplemented iso-sensitest media. Aliquots were plated
452 out at intervals between 1 and 11 months; LAT2 was identified after 8 months of growth in iso-
453 sensitest (Supplemental Fig. S1B).
454
455 **DNA extraction for long-range PCR**
456 DNA extraction of *WT* derivatives was carried out using the Wizard Genomic DNA Purification kit
457 (Promega). In brief, 1 mL of overnight *S*. Typhi culture, was harvested. Cells were pre-lysed in 600 µL
458 of Nuclei Lysis Solution and incubated at 80 °C for 10 min. 3 µL of RNase A was added to the lysed
459 cells and incubated for a further 15 min at 37 °C. 220 µL Protein Precipitation Solution was added to
460 the lysed cells before being incubated on ice for 15 min. The precipitated protein was separated
461 from the nucleic acids by centrifuged at 13.2 rpm for 15 min. 650 µL of the supernatant was mixed
462 with 650 µL isopropanol before being centrifuged at 13.2 rpm for 15 min. The supernatant was
463 discarded and the pellet was washed with 1 mL of 70 % ethanol, before being centrifuged at 13.2
464 rpm for 15 min. The supernatant was discarded and the pellet was left to dry. The dried pellet was
465 resuspended in 45 µL of DNA rehydration solution.
466
467 **Long-range PCR for identification of genome structures**
468 The primer sequences and combinations for detecting specific *rrn* (Supplemental Table S1) were
469 designed using the program Primer3 Input 0.4.0 (http://frodo.wi.mit.edu/) and were synthesised by
470 Sigma-Aldrich. All primers were aligned to the whole genome sequence of CT18 (Parkhill et al.
471 2001)to ensure specificity and no other matches with more than 80 % similarity were found. To
472 ensure consideration of all options, every possible primer combination was used in 91 separate PCR

reactions. PCRs were performed on 1 µL of DNA with 2X Fideli Taq PCR Master Mix (USB), 0.7 µM forward primer and 0.7 µM reserve primer in a total volume of 12.5 µL. The PCR conditions were: pre-incubation at 95 °C for 30 sec, amplification for 27 cycles at 95 °C for 25 sec, 59 °C for 1 min and 68 °C for 7 min, with a final extension at 68 °C for 7 min. Resulting *rrn* PCR products were separated out on 1 % agarose gels, before being detected using ethidium bromide staining (3 mg/mL).

DNA extraction for sequencing

DNA extraction of *S*. Typhi isolates was carried out using a modified protocol of the PuriSpin Fire Monkey kit (RevoluGen). In brief, 1 mL of overnight *S*. Typhi culture, was harvested. Cells were pre-lysed in 100 µL of 3 mg/mL lysozyme, 1.2 % Triton X-100, and incubated at 37 °C, 180 rpm for 10 min. 300 µL lysis solution (LSDNA, RevoluGen) and 20 µL of 20 mg/mL Proteinase K (Qiagen) was added to the partly-lysed cells and incubated at 56 °C for 20 min. 10 µL of 20 µg/µL RNase A (Sigma) was added to the lysed cells and incubated for a further 10 min at 37 °C. 350 µL binding solution (BS, RevoluGen) and 400 µL 75 % isopropanol was added to the lysed cells before they were transferred to the spin column. Bound DNA was washed as per manufacturer's instructions before being eluted in 2x100 µL of elution buffer (EB, RevoluGen) that had been pre-warmed at 65 °C. DNA concentration was determined using the broad range dsDNA assay kit (Thermo Fisher) on a Qubit 3.0 Fluorometer (Thermo Fisher). The quality of high-molecular weight DNA were assessed using the TapeStation 2200 (Agilent Technologies) automated electrophoresis platform with Genomic ScreenTape (Agilent Technologies) and a DNA ladder (200 to >60,000 bp, Agilent Technologies).

Long-read sequencing

MinION libraries, containing 6/12 DNA samples, were prepared using the Rapid Barcoding Kit (SQK-RBK004, ONT) as per the manufacturer's protocol. A pre-concentration step of 0.6x AMPure XP beads (Beckman Coulter) was performed on DNA samples which did not meet the manufacturer's DNA input recommendations (400 ng in 7.5 µL). The library was loaded onto the flow cell according

499 to the manufacturer's instructions. Sequencing was performed on the MinION platform using R9.4
500 flow cells (FLO-MIN106, ONT) with a run time of up to 120 hrs. ONT MinKNOW software v1.4 was
501 used to collect raw sequencing data and ONT Guppy v2.3.7 was used for local base-calling of the raw
502 data after sequencing runs were completed. Python qcat command was used to de-multiplex
503 samples.
504
505 **Short-read sequencing**
506 Genomic DNA was normalised to 0.5 ng/µL with EB (10 mM Tris-HCl). 0.9 µL of TD Tagment DNA
507 Buffer (Illumina Catalogue No. 15027866) was mixed with 0.09 µL TDE1, Tagment DNA Enzyme
508 (Illumina Catalogue No. 15027865) and 2.01 µL PCR grade water in a master mix and 3 µL added to a
509 chilled 96 well plate. 2 µL of normalised DNA (1 ng total) was pipette mixed with the 3 µL of the
510 tagmentation mix and heated to 55 ^{o}C for 10 min in a PCR block. A PCR master mix was made up
511 using 4 µL kapa2G buffer, 0.4 µL dNTPs, 0.08 µL Polymerase and 6.52 µL PCR grade water, contained
512 in the Kap2G Robust PCR kit (Sigma Catalogue No. KK5005) per sample and 11 µL added to each well
513 need to be used in a 96-well plate. 2 µL of each P7 and P5 of Nextera XT Index Kit v2 index primers
514 (Illumina Catalogue No. FC-131-2001 to 2004) were added to each well. Finally, the 5 µL of
515 Tagmentation mix was added and mixed. The PCR was run with 72 ^{o}C for 3 min, 95 ^{o}C for 1 min, 14
516 cycles of 95 ^{o}C for 10 s, 55 ^{o}C for 20 s and 72 ^{o}C for 3 min. Following the PCR reaction the libraries
517 were quantified using the Quant-iT dsDNA Assay Kit, high sensitivity kit (Catalogue No. 10164582)
518 and run on a FLUOstar Optima plate reader. Libraries were pooled following quantification in equal
519 quantities. The final pool was double-SPRI size selected between 0.5 and 0.7X bead volumes using
520 KAPA Pure Beads (Roche Catalogue No. 07983298001). The final pool was quantified on a Qubit 3.0
521 instrument and run on a High Sensitivity D1000 ScreenTape (Agilent Catalogue No. 5067-5579) using
522 the Agilent Taestation 4200 to calculate the final library pool molarity.
523

The pool was run at a final concentration of 1.8 pM on an Illumina Nextseq500 instrument using a Mid Output Flowcell (NSQ® 500 Mid Output KT v2(300 CYS) Illumina Catalogue FC-404-2003) following the Illumina recommended denaturation and loading recommendations which included a 1 % PhiX spike in (PhiX Control v3 Illumina Catalogue FC-110-3001). Data was uploaded to Basespace (www. basespace.illumina.com) where the raw data was converted to 2 FASTQ files for each sample.

Long-read and hybrid assemblies bioinformatics workflow

Bioinformatic analysis was performed on the open platform Galaxy. Prior to assembly, two steps were included to trim nanopore data. Filtlong v0.2.0 (https://github.com/rrwick/Filtlong) was used to trim nanopore data and only keep reads over 1 kb with a minimum mean quality score of 50. Porechop v0.2.3 (https://github.com/rrwick/Porechop) was used to remove sequencing adapters in the middle or the ends of each read. The long-read sequence correction and assembly tool Flye v2.5 (Kolmogorov et al. 2019) was used to assemble reads into contigs using an estimated genome size of 5 Mb. This long-read assembly was then polished with two rounds of Racon v1.3.1.1 (Vaser et al. 2017) and one round of Medaka v0.11.5 (ONT) using trimmed long-read data and corresponding overlapped reads generated by Minimap2 v2.12 (Li 2018). Hybrid assemblies were then generated by further polishing the final long-read assembly with two rounds of Pilon v1.20.1 (Walker et al. 2014) using short-read data and corresponding overlapped reads generated by Minimap2 v2.12 (Li 2018). Assemblies were evaluated for completeness and contamination with CheckM v1.0.11 (Parks et al. 2015).

GSs of isolates were then identified using two methods. Automatic identification of genome structure was performed by *socru* v2.2.2 (Page et al. 2020). Manual determination of genome order and fragment orientation was performed using Artemis Comparison Tool v18.0.2 (Carver et al. 2008) after annotation of the *rrn* operons with Prokka v1.14.5 (Seemann 2014). Within both methods, assembled genomic reads were aligned to the reference genome of *S*. Typhimurium LT2 which acted

as a baseline for genome order and fragment orientation.

Nucleotide variation analysis

Short-read data for WT and variants were analysed using the program breseq v0.24.0+2 (Deatherage and Barrick 2014), which outputs a list of probable mutations of various types and the sequence evidence for them. All analysis were run in consensus mode against the Ty2 reference sequence (RefSeq assession number NC_004631.1). Nucleotide variations which were common to WT and all variants, including deletions associated with the attenuation of WT strain, were not included in any further analysis. SNPs were checked using Snippy and Snippy-core v4.4.3 (https://github.com/tseemann/snippy). Large deletions (greater than 10 bp) were checked in Artemis Comparison Tool v18.0.2 (Carver et al. 2008).

Original growth curve analysis of WT derivatives

Growth curves were generated by growing strains in triplicate in isosensitest broth at 37 °C with agitation. Overnight cultures were used to inoculate 200 µL isosensitest broth to an OD_{600} of ~0.1 before OD readings were taken every 10 min over 11 hrs with a Fluostar Optima Microplate Reader (BMG Labtech).

Repeated growth curve analysis of WT derivatives

Growth curves were generated by growing strains in triplicate in no salt LB broth at 37 °C with agitation. Overnight cultures were then standardised to an OD_{600} of ~0.6, before a further 100X dilution was made. OD readings were taken every 15 min for 100 µL prepared cultures over 11 hrs with a Bioscreen C plate reader (Growth Curves Ltd). The growth rate was graphically determined by fitting a straight line on the exponential phase of the growth curve and calculating its slope.

RNA extraction

RNA extraction of *S*. Typhi isolates was carried out, in triplicate for each isolate, using the All Prep DNA/RNA Mini extraction kit (Qiagen) following manufactures protocol. In brief, 100 µL of overnight culture was used to inoculate 10 mL EZ-media before being incubated at 37 °C, 180 rpm until an OD of ~0.35-0.40 was reached (~4 hrs). Cells were harvested by centrifugation at 4,000 g for 10 min and then resuspended in 100 µL RNAlater RNA stabilization reagent (Thermo Fisher). 600 µL buffer RLT Plus was added to the cell suspension before being pipetted mixed and transferred to an AllPrep RNA spin column. One volume (700 µL) of 70% ethanol was added to the flow-through before being pipette mixed and transferred to an AllPrep RNeasy spin. Bound RNA was washed as per manufacturer's instructions before being eluted in 2x30 µL of RNAse-free water. RNA concentration was determined using the high sensitivity RNA assay kit (Thermo Fisher) on a Qubit 3.0 Fluorometer (Thermo Fisher). The quality of RNA were assessed using the TapeStation 2200 (Agilent Technologies) automated electrophoresis platform with RNA ScreenTape (Agilent Technologies) and a DNA ladder (50 to >6,000 bp, Agilent Technologies).

RNAseq library preparation

From total RNA, the ribosomal RNA was depleted with the RiboCop rRNA Depletion Kit for Bacteria (Lexogen) using the Gram-negative (G-) probe mix according to the manufacturer's protocol. RNAseq library preparation was carried out using a modified protocol of the QIAseq Stranded mRNA Select kit (Qiagen), which in brief used a fifth of the RNA input and reagents. The quality of RNAseq library were assessed using the TapeStation 2200 (Agilent Technologies) automated electrophoresis platform with D5000 ScreenTape (Agilent Technologies) and a DNA ladder (100 to 5,000 bp, Agilent Technologies). RNAseq librabries were sequenced on the Nextseq500 (Illumina) using a Mid Output Flowcell with the aim of obtaining 10 million reads per replicate (~X2000 gene coverage). Data was uploaded to Basespace (www. basespace.illumina.com) where the raw data was converted to 2 FASTQ files for each sample.

Differentially expressed gene analysis

Bioinformatic analysis was performed on the open platform Galaxy v19.05. The quality of raw sequences was ascertained using FastQC v0.72 (https://github.com/s-andrews/FastQC) before being quality control trimmed using fastp v0.19.5 (Chen et al. 2018). HISAT2 v2.1.0 (Kim et al. 2015) was used to align reads to the Ty2 reference sequence (RefSeq assession number NC_004631.1). Assignment of aligned reads to the genes of Ty2 was measured using featureCounts v1.6.3 (Liao et al. 2014) before DESeq2 v2.11.40.4 (Love et al. 2014), which is designed for the use with biological replicates, was used to determine differentially expressed genes from the count tables. The corrected p-value (p-adj), which is adjusted for multiple testing and controls the false discovery rate, was used to screen the DEGs. p-adj ≤ 0.05 was set as the threshold to judge significance of differential gene expression. After identifying significant DEGs, these were further screened using the absolute log2 fold change which was set to lLog2FCl ≥ 0.58, which is equivalent to lFCl ≥ 1.5, to judge the magnitude of the expression change.

Brig v0.95 (Alikhan et al. 2011) was used as a way to visualise the significant DEGs on a global scale using the parent WT genome, cut at dnaA to allow dnaA to be the beginning of the genome, as the backbone reference genome. The fragments of the parent and variate GSs were plotted as the first and second rings respectively to indicate the fragments involved in the genome rearrangement.

PMA_{xx} real-time PCR bacterial viability test

A PMA_{xx} Real-Time PCR Bacterial Viability Test (Biotium Inc.), designed for selective detection of viable *S. enterica* cells in the presence of dead bacteria, was used to determine if any of the cells within a glycerol stock of isolate T were viable even though it was no longer culturable. See supplementary material.

Data Access

The Illumina and nanopore genome sequence data, RNA-seq data and hybrid assemblies generated in this study are available in DDBJ/ENA/GenBank databases under the Project accession number PRJEB52538 and per sample as: ERS11885537 (WT), ERS11885538 (7), ERS11885539 (8), ERS11885540 (U), ERS11885541 (T), ERS11885542 (ISO T), ERS11885543 (EZ T) and ERS11885544 (LAT2).

Competing Interest Statement

GCL has previously consulted for RevoluGen Ltd on bioinformatic analyses. Fire Monkey DNA extraction kits were provided free of charge by RevoluGen in this project.

Acknowledgments

The authors would like to thank Dave Baker and the QIB sequencing facility for support in Illumina DNA and RNA sequencing, Gemma Kay for advice in MinION setup and Satheesh Nair and Keith Turner for useful discussions on long range PCR.

EVW, JW and GCL gratefully acknowledge the support of the Biotechnology and Biological Sciences Research Council (BBSRC); this research was funded by the BBSRC Institute Strategic Programme Microbes in the Food Chain BB/R012504/1 and its constituent project BBS/E/F/000PR10349.

Author contributions

EVW – Methodology, validation, investigation, formal analysis, visualisation, writing original draft, review and editing. LAT – Validation, investigation, formal analysis. JKA – Methodology, validation, investigation. JW – Conceptualisation, writing - review and editing. GCL – Conceptualisation, data curation, visualisation, writing original draft, review and editing.

Supplemental Material

Supplemental Methods, Supplemental Figures S1-S7 and Supplemental Tables S1-S2

Supplemental Table S3: RNAseq

Supplemental Table S4: Significant differentially expressed genes

References

Achaz G, Rocha EPC, Netter P, Coissac E. 2002. Origin and fate of repeats in bacteria. *Nucleic Acids Res* **30**: 2987–2994. doi:10.1093/nar/gkf391.

Alikhan NF, Petty NK, ben Zakour NL, Beatson SA. 2011. BLAST Ring Image Generator (BRIG): simple prokaryote genome comparisons. *BMC Genom* **12**: 1–10. doi:10.1186/1471-2164-12-402.

Arredondo-Alonso S, Pöntinen AK, Cléon F, Gladstone RA, Schürch AC, Johnsen PJ, Samuelsen Ø, Corander J. 2021. A high-throughput multiplexing and selection strategy to complete bacterial genomes. *Gigascience* **10**: 1–13. doi:10.1093/gigascience/giab079.

Blom J, Kreis J, Spänig S, Juhre T, Bertelli C, Ernst C, Goesmann A. 2016. EDGAR 2.0: an enhanced software platform for comparative gene content analyses. *Nucleic Acids Res* **44**: W22–W28. doi:10.1093/NAR/GKW255.

Brüssow H, Canchaya C, Hardt W-D. 2004. Phages and the evolution of bacterial pathogens: from genomic rearrangements to lysogenic conversion. *Microbiol Mol Biol Rev* **68**: 560–602. doi:10.1128/MMBR.68.3.560-602.2004.

Carver T, Berriman M, Tivey A, Patel C, Böhme U, Barrell BG, Parkhill J, Rajandream MA. 2008. Artemis and ACT: viewing, annotating and comparing sequences stored in a relational database. *Bioinformatics* **24**: 2672–2676. doi:10.1093/bioinformatics/btn529.

Casino P, Miguel-Romero L, Huesa J, García P, García-del Portillo F, Marina A. 2018. Conformational dynamism for DNA interaction in the *Salmonella* RcsB response regulator. *Nucleic Acids Res* **46**: 456–472. doi:10.1093/nar/gkx1164.

Chen S, Zhou Y, Chen Y, Gu J. 2018. fastp: an ultra-fast all-in-one FASTQ preprocessor. *Bioinformatics* **34**: i884–i890. doi:10.1093/bioinformatics/bty560.

Darling AE, Mau B, Perna NT. 2010. progressiveMauve: multiple genome alignment with gene gain, loss and rearrangement. *PLoS One* **5**: e11147. doi:10.1371/journal.pone.0011147.

Darling AE, Miklós I, Ragan MA. 2008. Dynamics of genome rearrangement in bacterial populations. *PLoS Genet* **4**: e1000128. doi:10.1371/journal.pgen.1000128.

Deatherage DE, Barrick JE. 2014. Identification of mutations in laboratory evolved microbes from next-generation sequencing data using *breseq*. *Methods Mol Biol* **1151**: 165–188. doi:10.1007/978-1-4939-0554-6_12.

Deng W, Liou S-R, Plunkett G, Mayhew GF, Rose DJ, Burland V, Kodoyianni V, Schwartz DC, Blattner FR. 2003. Comparative genomics of *Salmonellaenterica* serovar Typhi strains Ty2 and CT18. *J Bacteriol* **185**: 2330–2337. doi:10.1128/JB.185.7.2330-2337.2003.

Fitzgerald SF, Lupolova N, Shaaban S, Dallman TJ, Greig D, Allison L, Tongue SC, Evans J, Henry MK, McNeilly TN, et al. 2021. Genome structural variation in *Escherichia coli* O157:H7. *Microb Genom* **7**: 1–18. doi:10.1099/mgen.0.000682.

Guan H-H, Yoshimura M, Chuankhayan P, Lin C-C, Chen N-C, Yang M-C, Ismail A, Fun H-K, Chen C-J. 2015. Crystal structure of an antigenic outer-membrane protein from *Salmonella* Typhi suggests a potential antigenic loop and an efflux mechanism. *Sci Rep* **5**: 1–12. doi:10.1038/srep16441.

Guerrero P, Collao B, Álvarez R, Salinas H, Morales EH, Calderón IL, Saavedra CP, Gil F. 2013. *Salmonella enterica* serovar Typhimurium BaeSR two-component system positively regulates *sodA* in response to ciprofloxacin. *Microbiology* **159**: 2049–2057. doi:10.1099/mic.0.066787-0.

Hars U, Horlacher R, Boos W, Welte W, Diederichs K. 1998. Crystal structure of the effector-binding domain of the trehalose-repressor of *Escherichia coli*, a member of the LacI family, in its complexes with inducer trehalose-6-phosphate and noninducer trehalose. *Protein Sci* **7**: 2511–2521. doi:10.1002/pro.5560071204.

Hughes D. 2000. Evaluating genome dynamics: the constraints on rearrangements within bacterial genomes. *Genome Biology* **1**: 1–8. doi:10.1186/gb-2000-1-6-reviews0006.

Kim D, Langmead B, Salzberg SL. 2015. HISAT: a fast spliced aligner with low memory requirements. *Nature Methods* **12**: 357–360. doi:10.1038/nmeth.3317.

Kolmogorov M, Yuan J, Lin Y, Pevzner PA. 2019. Assembly of long, error-prone reads using repeat graphs. *Nat Biotechnol* **37**: 540–546. doi:10.1038/s41587-019-0072-8.

Koskiniemi S, Sun S, Berg OG, Andersson DI. 2012. Selection-driven gene loss in bacteria. *PLoS Genet* **8**: e1002787. doi:10.1371/journal.pgen.1002787.

Kothapalli S, Nair S, Alokam S, Pang T, Khakhria R, Woodward D, Johnson W, Stocker BAD, Sanderson KE, Liu S-L. 2005. Diversity of genome structure in *Salmonella enterica* serovar Typhi populations. *J Bacteriol* **187**: 2638–2650. doi:10.1128/JB.187.8.2638-2650.2005.

Langridge GC, Phan M-D, Turner DJ, Perkins TT, Parts L, Haase J, Charles I, Maskell DJ, Peters SE, Dougan G, et al. 2009. Simultaneous assay of every *Salmonella Typhi* gene using one million transposon mutants. *Genome Res* **19**: 2308–2316. doi:10.1101/gr.097097.109.

Lee H, Doak TG, Popodi E, Foster PL, Tang H. 2016. Insertion sequence-caused large-scale rearrangements in the genome of *Escherichia coli*. *Nucleic Acids Res* **44**: 7109–7119. doi:10.1093/nar/gkw647.

Li H. 2018. Minimap2: pairwise alignment for nucleotide sequences. *Bioinformatics* **34**: 3094–3100. doi:10.1093/bioinformatics/bty191.

Liao Y, Smyth GK, Shi W. 2014. featureCounts: an efficient general purpose program for assigning sequence reads to genomic features. *Bioinformatics* **30**: 923–930. doi:10.1093/bioinformatics/btt656.

Liu S-L, Sanderson KE. 1996. Highly plastic chromosomal organization in *Salmonella typhi*. *Proc Natl Acad Sci U S A* **93**: 10303–10308. doi:10.1073/pnas.93.19.10303.

Liu S-L, Sanderson KE. 1998. Homologous recombination between *rrn* operons rearranges the chromosome in host-specialized species of *Salmonella*. *FEMS Microbiol Lett* **164**: 275–281. doi:10.1016/S0378-1097(98)00225-0.

Love MI, Huber W, Anders S. 2014. Moderated estimation of fold change and dispersion for RNA-seq data with DESeq2. *Genome Biology* **15**: 1–21. doi:10.1186/s13059-014-0550-8.

Matthews TD, Rabsch W, Maloy S. 2011. Chromosomal Rearrangements in *Salmonella enterica* Serovar Typhi Strains Isolated from Asymptomatic Human Carriers. *mBio* **2**: e00060-11. doi:10.1128/mbio.00060-11.

Nakagawa I, Kurokawa K, Yamashita A, Nakata M, Tomiyasu Y, Okahashi N, Kawabata S, Yamazaki K, Shiba T, Yasunaga T, et al. 2003. Genome sequence of an M3 strain of *Streptococcus pyogenes* reveals a large-scale genomic rearrangement in invasive strains and new insights into phage evolution. *Genome Res* **13**: 1042–1055. doi:10.1101/gr.1096703.

Nikaido E, Yamaguchi A, Nishino K. 2008. AcrAB multidrug efflux pump regulation in *Salmonella enterica* serovar Typhimurium by RamA in response to environmental signals. *J Biol Chem* **283**: 24245–24253. doi:10.1074/jbc.M804544200.

Page AJ, Ainsworth EV, Langridge GC. 2020. *socru*: typing of genome-level order and orientation around ribosomal operons in bacteria. *Microb Genom* **6**: 1–6. doi:10.1099/mgen.0.000396.

Parkhill J, Dougan G, James KD, Thomson NR, Pickard D, Wain J, Churcher C, Mungall KL, Bentley SD, Holden MTG, et al. 2001. Complete genome sequence of a multiple drug resistant *Salmonella enterica* serovar Typhi CT18. *Nature* **413**: 848–852. doi:10.1038/35101607.

748 Parks DH, Imelfort M, Skennerton CT, Hugenholtz P, Tyson GW. 2015. CheckM: assessing the quality
749 of microbial genomes recovered from isolates, single cells, and metagenomes. *Genome Res* **25**:
750 1043–1055. doi:10.1101/gr.186072.114.
751 Seemann T. 2014. Prokka: rapid prokaryotic genome annotation. *Bioinformatics* **30**: 2068–2069.
752 doi:10.1093/bioinformatics/btu153.
753 Tacket CO, Sztein MB, Losonsky GA, Wasserman SS, Nataro JP, Edelman R, Pickard D, Dougan G,
754 Chatfield SN, Levine MM. 1997. Safety of live oral *Salmonella* typhi vaccine strains with
755 deletions in *htrA* and *aroC aroD* and immune response in humans. *Infect Immun* **65**: 452–456.
756 doi:10.1128/iai.65.2.452-456.1997.
757 Turner AK, Nair S, Wain J. 2006. The acquisition of full fluoroquinolone resistance in *Salmonella*
758 Typhi by accumulation of point mutations in the topoisomerase targets. *J. Antimicrob.*
759 *Chemother.* **58**: 733–740. doi:10.1093/jac/dkl333.
760 Tyson JR, James P, Stoddart D, Sparks N, Wickenhagen A, Hall G, Choi JH, Lapointe H, Kamelian K,
761 Smith AD, et al. 2020. Improvements to the ARTIC multiplex PCR method for SARS-CoV-2
762 genome sequencing using nanopore. *bioRxiv*. doi:10.1101/2020.09.04.283077.
763 Vanaporn M, Titball RW. 2020. Trehalose and bacterial virulence. *Virulence* **11**: 1192–1202.
764 doi:10.1080/21505594.2020.1809326.
765 Vaser R, Sović I, Nagarajan N, Šikić M. 2017. Fast and accurate de novo genome assembly from long
766 uncorrected reads. *Genome Res* **27**: 737–746. doi:10.1101/gr.214270.116.
767 Virlogeux I, Waxin H, Ecobichon C, Lee JO, Popoff MY. 1996. Characterization of the *rcsA* and *rcsB*
768 Genes from *Salmonella typhi*: *rcsB* through *tviA* Is Involved in Regulation of Vi Antigen
769 Synthesis. *J Bacteriol* **178**: 1691–1698. doi:10.1128/jb.178.6.1691-1698.1996.
770 Walker BJ, Abeel T, Shea T, Priest M, Abouelliel A, Sakthikumar S, Cuomo CA, Zeng Q, Wortman J,
771 Young SK, et al. 2014. Pilon: an integrated tool for comprehensive microbial variant detection
772 and genome assembly improvement. *PLoS One* **9**: e112963. doi:10.1371/journal.pone.0112963.
773 Wall E, Majdalani N, Gottesman S. 2018. The complex Rcs regulatory cascade. *Annu Rev Microbiol*
774 **72**: 111–139. doi:10.1146/annurev-micro-090817-062640.
775 Weigand MR, Peng Y, Batra D, Burroughs M, Davis JK, Knipe K, Loparev VN, Johnson T, Juieng P,
776 Rowe LA, et al. 2019. Conserved patterns of symmetric inversion in the genome evolution of
777 *Bordetella* respiratory pathogens. *mSystems* **4**: e00702-19. doi:10.1128/msystems.00702-19.
778 Weigand MR, Peng Y, Loparev V, Batra D, Bowden KE, Burroughs M, Cassiday PK, Davis JK, Johnson T,
779 Juieng P, et al. 2017. The history of *Bordetella pertussis* genome evolution includes structural
780 rearrangement. *J Bacteriol* **199**: e00806-16. doi:10.1128/JB.00806-16.
781